

Optical modeling and measurements of a coccolithophore bloom

Timothy J. Smyth, Gerald F. Moore, Stephen B. Groom, Peter E. Land, and Toby Tyrrell

Blooms of the phytoplankton coccolithophorid *Emiliana huxleyi* can cause significant changes to both the inherent and the apparent optical properties within an oceanic column. Measurements made within such a bloom off the southwestern coast of England during July 1999 are reported. The multiple scattering properties of the bloom prevented accurate retrieval of absorption (a) and attenuation (c) coefficients with a WETLabs ac-9. Upwelling radiance measurements were similarly affected by the bloom, which caused the sensors to saturate. An optical model has been developed that gives close agreement with the *in situ* optics when it is used as input to the Hydrolight radiative-transfer model.

© 2002 Optical Society of America

OCIS codes: 010.4450, 280.0280.

1. Introduction

Following a period of warm settled conditions during July 1999, a large bloom of the coccolithophorid *Emiliana huxleyi* formed in waters off the southwestern coast of England. The bloom at its greatest extent covered approximately 16,000 km² and lasted for 3 weeks, until it was dispersed by more unsettled weather conditions during August. Coccolithophores are phytoplankton that synthesize external calcium carbonate platelets (coccoliths, or liths): During the latter stages of a bloom these coccoliths are shed in large numbers, giving the water a turquoise–white appearance, which is easily detectable both at the surface and from space. Our aim with this paper is twofold: first to develop an inherent optical property (IOP) model that includes the effects of *E. huxleyi* and second to investigate the optical behavior of coccoliths by use of an intercomparison between modeling and *in situ* measurements.

2. Method

On 30 July 1999, samples in and close to the bloom were taken aboard the RV Squilla. Throughout

the duration of the sampling campaign there were cloudless skies and light winds; atmospheric haze restricted visibility to ~10 km within the bloom. The optical measurements, following strict Sea-viewing Wide Field-of-view Sensor (SeaWiFS) protocols,¹ were taken with a multispectral radiometer profiler. The radiometers attached to the profiling rig were engineered by SEI Satlantic: downwelling irradiance and upwelling radiance were measured at 412, 443, 490, 510, 555, 620 and 665 nm. A WETLabs ac-9 was also attached to the profiling rig to measure absorption (a) and attenuation (c) at 412, 440, 488, 510, 555, 630, 650, 676 and 715 nm. A deck cell which measured above-water downwelling irradiance at the same wavelengths as the radiometers, was permanently attached above cabin level toward the bow of the boat.

A total of four combined optical and ac-9 stations was established; we made the first cast (at station 1; see Fig. 1) in a region deemed, from onboard transmissometer readings, to be outside the region of the bloom in an attempt to determine the background characteristics. However, from the satellite imagery shown in Fig. 1 it is evident that station 1 was not completely outside the influence of the bloom. This conclusion is further corroborated by Fig. 2, which shows the presence of liths, albeit at a much reduced concentration, throughout the water column at station 1. At station 3 the optical measurements were timed to coincide with the overpass of the SeaWiFS ocean color satellite shown in Fig. 1.

T. J. Smyth (e-mail: tjsm@pml.ac.uk), G. F. Moore, S. B. Groom, and P. E. Land are with the Plymouth Marine Laboratory, Prospect Place, Plymouth, Devon, PL1 3DH, UK. T. Tyrrell is with the School of Ocean and Earth Science, Southampton Oceanography Centre, University of Southampton, Southampton, UK.

Received 17 April 2002; revised manuscript received 3 September 2002.

0003-6935/02/367679-10\$15.00/0

© 2002 Optical Society of America

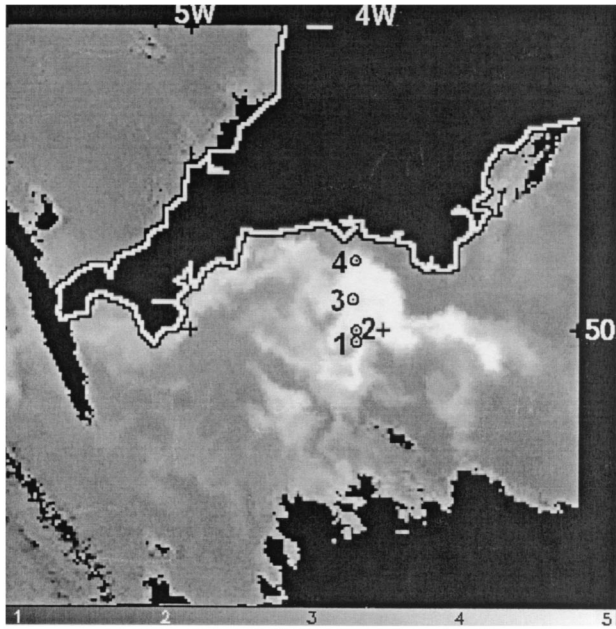


Fig. 1. Measured normalized water-leaving radiance at 555 nm [$L_{wn}(555)$] for the SeaWiFS overpass at 1251 GMT on 30 July 1999, showing the location and extent of the coccolithophore bloom. The locations of the various sampling stations are marked.

A. Optics Theory

The normalized water-leaving radiance² (L_{wn}) is a standard SeaWiFS product and can be calculated from the optics data with the following equation:

$$L_{wn}(\lambda) = L_u(0^-, \lambda) \frac{1 - \rho(\lambda, \theta)}{n_w^2(\lambda)} \times \frac{\overline{E_0(\lambda)}}{E_s(\lambda)} \quad [\text{mW cm}^{-2} \text{sr}^{-1} \mu\text{m}^{-1}], \quad (1)$$

where $L_u(0^-, \lambda)$ is the subsurface upwelling radiance calculated from the optical profiler measurements and $E_s(\lambda)$ is the downwelling solar irradiance measured by the deck cell. $L_u(0^-, \lambda)$ is determined by a linear regression of the natural logarithm of $L_u(\lambda)$ against depth to extrapolate to the sea surface; the values of $E_s(\lambda)$ are smoothed values of the deck cell data from a moving window of 32 data points, or 10 s. $\overline{E_0(\lambda)}$ is the mean extraterrestrial solar irradiance³ and $\rho(\lambda, \theta)$ and $n_w(\lambda)$ are the Fresnel reflectance and the refractive index, respectively, of sea water.

The diffuse attenuation coefficient for downwelling irradiance, $K_d(z, \lambda)$, can be determined from the optical measurements from

$$K_d(z, \lambda) = -\frac{d \ln E_d(z, \lambda)}{dz} \quad [\text{m}^{-1}] \quad (2)$$

and can be obtained at each wavelength by regression of the natural logarithm of the irradiance against depth over an interval where there is little deviation from the exponential decay profile. K_d has implications for remote sensing, as ~90% of the water-

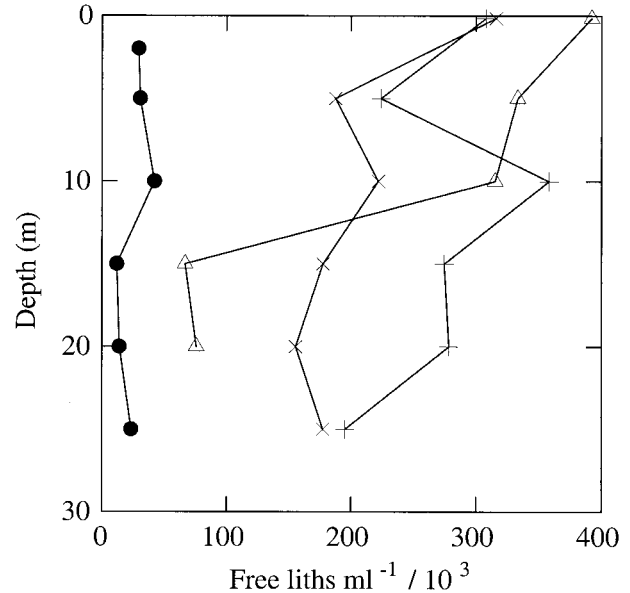


Fig. 2. Variation of the number of liths within the coccolithophore bloom at station 1 (filled circles), station 2 (crosses), station 3 (pluses), and station 4 (open triangles) measured by flow cytometry.

leaving radiance comes from a surface layer of depth $1/K_d$.⁴

B. ac-9 Measurements

The ac-9 consists of upper and lower pressurized canisters separated by a pathlength of 0.25 m over which spectral absorption (a) and attenuation (c) are determined.⁵ The lower canister houses a tungsten lamp, discriminated spectrally by nine bandpass filters, and the transmitter optics for the a and c channels. The upper canister contains the a detector and the c receiver. Between the two canisters there are two removable plastic flow assemblies that contain the measurement volumes for absorbance and transmittance. The data from the ac-9 instrument were processed with the WETView software package, which converts the raw binary data into inverse meters and then applies temperature and clean-water corrections. Further corrections were made to the absorption data to account for the temperature and salinity differences between the optically pure reference water and the water within which the measurements were taken. Scattering corrections were applied to the absorption data according to manufacturer protocols that allowed for changes in the spectral scattering correction magnitude and in the types of material present. Finally, we added the pure-water absorption^{6,7} and attenuation⁸ coefficients to obtain the total absorption and attenuation coefficient values.

C. Modeling

Previous optical modeling studies of coccolithophore blooms have included a multispectral, multicomponent Monte Carlo approach⁹ and a coupled atmo-

sphere and ocean radiative-transfer model.¹⁰ In this paper a modified version of the model of Sathyendranath *et al.*¹¹ (MSM) was used as input to an in-water numerical radiative-transfer code.

1. Implementation of the Sathyendranath Model

The Sathyendranath model was modified to include backscattering by coccolithophores. Equation (5) of Ref. 11 thus becomes

$$b_b(\lambda) = b_{bw}(\lambda) + b_{bp}(\lambda) + b_{bcoccolith}(\lambda) + b_{bcell}(\lambda) \quad [\text{m}^{-1}], \quad (3)$$

where b_b is the total backscatter, b_{bw} is the backscatter that is due to pure seawater, b_{bp} is the backscatter that is due to (noncoccolith) particulate matter, and b_{bcocco} and b_{bcell} identify backscatter caused by the various *E. huxleyi* components. This separate treatment of detached coccoliths and cells was first applied by Ackleson *et al.*¹⁰ The coccolithophore-specific constants used in Ref. 10 were derived from data obtained from measurements made in the Gulf of Maine during coccolithophore blooms and are quoted in this paper as a comparison to indicate the range of values reported in the literature. Scattering by water was computed by¹²

$$b_{bw}(\lambda) = 0.5 \times 0.00288(\lambda/500)^{-4.32} \quad [\text{m}^{-1}]. \quad (4)$$

Scattering by particles (b_p) was modeled following the equations¹¹

$$b_p(660) = 0.407C^{0.795} \quad [\text{m}^{-1}], \quad (5)$$

$$b_p(\lambda) = b_p(660)(660/\lambda)^{\log_{10} C} \quad [\text{m}^{-1}], \quad (6)$$

$$b_{bp}(\lambda) = 0.01(0.78 - 0.42 \log_{10} C)b_p(\lambda) \quad [\text{m}^{-1}], \quad (7)$$

where C is the chlorophyll- a concentration in milligrams per cubic meter (mg m^{-3}). The backscatter that is due to coccoliths is modeled with¹³

$$b_{bcoccolith}(\lambda) = 10^6 N_{cocco} b_{bcoccolith}^*(546) (\lambda/546)^{-1.35} \quad [\text{m}^{-1}], \quad (8)$$

where N_{cocco} is the number of coccoliths per milliliter measured by flow cytometry and $b_{bcoccolith}^*(546)$ is a constant¹⁴ of 1.1×10^{-13} (Ref. 10 has constant of 1.17×10^{-13} and a wavelength exponent of -1.45). Using a combination of Eq. (3)–(8) results in a final expression for the total scattering (i.e., forward and back):

$$b(\lambda) = 2b_{bw}(\lambda) + b_p(\lambda) + 58b_{bcoccolith}(\lambda) \quad [\text{m}^{-1}], \quad (9)$$

where the multiplying factor ($b:b_b$ ratio) of 58 is determined at 546 nm by linear interpolation from previously published values⁹; i.e., the coccolith backscatter is approximately 2% of the forward scatter. Reference 10 gives a multiplying factor of 23 ($1/0.043$), which we derived by evaluating Eq. (14) of Ref. 10 at 660 nm. The Petzold¹⁵ scattering phase function has a $b:b_b$ ratio of 50; Tyrrell *et al.*,⁹ from

Table 1. Values of a_m^a and a_m^{*b} for a Curve Fitted to a Plot of Phytoplankton Absorption versus Chlorophyll- a

Wavelength (nm)	a_m (m^{-1})	a_m^* [$\text{m}^2/\text{mg}(\text{Chl})$]
412	1.1213	0.0591
440	1.016	0.0773
443	1.007	0.0646
488	0.4662	0.0434
490	0.481	0.0420
510	0.629	0.0279
555	0.856	0.0105

^aAsymptotic maximum value of the absorption coefficient.

^bMaximum slope near the origin.

observations at 436 nm, give a ratio of 62; Balch *et al.*,¹⁶ a ratio of 53 at 546 nm. Therefore the $b:b_b$ ratio of 58 used here compares well with values quoted in the literature.

The absorption components were modeled as follows:

$$a(\lambda) = a_w(\lambda) + a_y(\lambda) + a_p(\lambda) \quad [\text{m}^{-1}], \quad (10)$$

where a_w is the absorption coefficient of pure water,⁶ a_y is the absorption that is due to *gelbstoff* (i.e., yellow substance) and a_p is the absorption that is due to particulates. The absorption that is due to the yellow substance was modeled as follows:

$$a_y(\lambda) = 0.8a_p(440)\exp[-0.014(\lambda - 440)] \quad [\text{m}^{-1}]. \quad (11)$$

We investigated the influence of color dissolved organic matter by varying parameter a_y and comparing the modeled L_{wn} at 412 and 443 nm over a chlorophyll range of 0–2 mg m^{-3} , using data from the SeaWiFS Bio-optical Algorithm Mini-workshop (SeaBAM)¹⁷ dataset. The best-fit value, used in Eq. (11), was 0.8. The absorption that is due to particulates was modeled from

$$a_p(\lambda) = \frac{a_m(\lambda)a_m^*(\lambda)C}{a_m(\lambda) + a_m^*(\lambda)C}, \quad (12)$$

where $a_m(\lambda)$ [m^{-1}] and $a_m^*(\lambda)$ [$\text{m}^2/\text{mg}(\text{Chl})$] are the asymptotic maximum value of the absorption coefficient and the maximum slope near the origin, respectively, of a curve fitted to a plot of phytoplankton absorption versus chlorophyll- a at each wavelength (see e.g., Fig. 2 of Ref. 11). Table 1 lists the spectral values of a_m and a_m^* that we used as a lookup table within the MSM; additional wavelengths were generated by linear interpolation.

The input parameters of the model were pigment concentration (chlorophyll- a , b , c) determined by high-performance liquid chromatography¹⁸ and the number of free liths and whole cells determined by flow cytometry. These parameters were measured at discrete depths (0, 5, 10, 15, 20, 25 m) at each of the four stations. The outputs of the model runs were absorption and attenuation at 412, 440, 488, 510, and 555 nm to correspond to wavelengths measured by

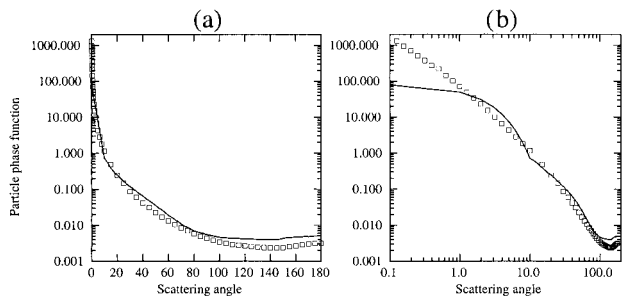


Fig. 3. Comparison of Petzold (open squares) and Voss (solid curves) particle phase function with (a) a linear and (b) a logarithmic abscissa to highlight changes at large and small angles, respectively.

the ac-9 so a direct comparison could be made. Wavelengths longer than 555 nm fell outside the spectral limits of the MSM and were therefore not modeled.

2. Determination of the Coccolithophore Phase Function

The scattering properties of a particle depend upon the particle's size and shape and the real components of its complex refractive index. Coccoliths are optically distinct from coccolithophores because they differ in both size and shape. As coccoliths (and to a lesser extent coccolithophores) are highly scattering, characterization of the phase function is important for accurate modeling of the effects on the in-water light field.

Coccoliths have been modeled as shapes including disks, washers, and fishing reels¹⁹ whose individual phase functions have many unrealistic oscillations that average out in b_b .²⁰ Thus one would be led to the conclusion that a phase function for coccolithophores is theoretically unattainable in part because of their shape and random orientation.

Figure 3 shows the Petzold phase function¹⁵ (open squares) and a phase function determined by volume scattering function measurements made by Voss at 10°–170° within a coccolithophore bloom.²¹ The Voss phase function below 10° was reconstructed by inspection to ensure that the backscattering probability, \tilde{b}_b , agreed with the measured estimates. It is at these angles (<10°) that there is a marked (order-of-magnitude) departure from the Petzold phase function in the forward direction. The Voss and the Petzold phase functions in the backward direction differ only slightly, certainly as a percentage of the total scattering. Because of the unreliability of the Voss phase function at small angles and the similarity between the Voss and the Petzold phase functions in the backscatter direction, the Petzold phase function is taken to be characteristic of the coccolithophore phase function.

3. Modeling the In-Water Light Field

The IOPs determined from the ac-9 instrument and the MSM were used as input into the Hydrolight v 3.0

numerical radiative-transfer code.²² We ran the model by using date, time, and position information for each of the four stations to calculate the solar zenith angle and clear-sky radiance information.²³ The water was radiatively partitioned into two components: pure water and particulate matter. In the scattering calculations the phase function of pure water¹⁵ was used for component 1 and the Petzold phase function was used for component 2. The model was run at 30 depths in the top 15 m of the water column for the five ac-9 wavelengths used in the MSM, which almost correspond to those of SeaWiFS, namely 412 and 440 (cf. 443 for SeaWiFS), 488 (cf. 490), 510 and 555 nm; the depth intervals were smaller toward the surface. The output downwelling irradiance [$E_d(\lambda)$], the upwelling radiance [$L_u(\lambda)$], and various apparent optical properties [e.g., $L_{wn}(\lambda)$ and $K_d(\lambda)$] were then compared with those measured with the Atlantic radiometers.

3. Results

A. Bloom Characteristics

The SeaWiFS image in Fig. 1 shows considerable structure within the coccolithophore bloom on a scale as small as 1.2 km. Small eddies can be seen in and near the bloom (e.g., at 49° 30'N and 3° 40'W). The white areas are regions populated by coccolithophores that are likely to have shed their chalky liths. The maximum above-water reflectance at 555 nm measured by SeaWiFS was ~12% (cf. 0.4% for the low-chlorophyll regions of the open ocean). Embedded within the coccolithophore bloom were red patches of *Gymnodinium mikimotoi*, which were observed by several mariners and were apparent in SeaWiFS color composite imagery (not shown). The black areas are masked out because of the presence of land or clouds.

Figure 2 shows the concentration of shed (free) liths, determined by flow cytometry,²⁴ at each station. Flow cytometry was used in preference to the traditional method of manual counting of samples fixed in buffered formalin because it was found that the fixation process actually caused the coccolithophores to shed their liths. This shedding gave as much as a twofold increase in the number of liths,²⁵ which would strongly influence the modeling of the light field described in this paper. We verified this observed shedding of liths within the preserved samples by comparing several fresh and preserved samples of cultures of *E. huxleyi*, using the flow cytometer. Results both from counts made of the coccolithophores²⁶ and from flow cytometry²⁵ showed that the bloom population was made up almost entirely of shed liths (the highest ratios measured were 4000 liths cell⁻¹). This is consistent with previous observations made within such blooms.^{9,27}

Figure 4 shows the variation in temperature and density (derived from the temperature and salinity fields) with depth within the coccolithophore bloom. Stations 1 and 2 are mixed in the upper layer, whereas stations 3 and 4 are stratified above 13 m.

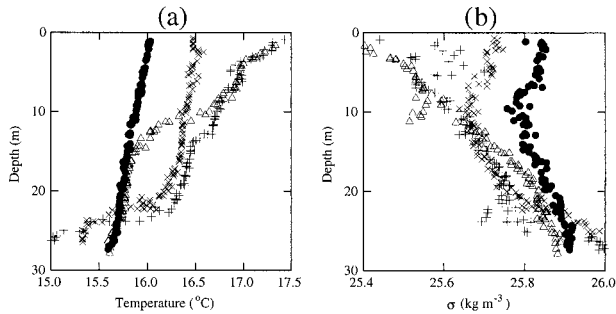


Fig. 4. Variation of (a) temperature and (b) density (σ_t) within the coccolithophore bloom at station 1 (filled circles), station 2 (crosses), station 3 (pluses), and station 4 (open triangles). Data taken by temperature and salinity sensors mounted on the optics rig were used.

Stations 1 and 4 have the same characteristics in temperature and density below 14 m, whereas 2 and 3 are physically alike below 23 m. These two types of profile cross at 23 m, which marks the position of the thermocline in stations 2 and 3. Stations 1 and 2 have an increase in salinity toward the surface, which possibly is due to evaporation, whereas stations 3 and 4 have decreased salinity toward the surface as a result of the influence of freshwater outflow from the river Tamar. In short, the bloom's physical environment was complex. The surface warming that strengthens with the progression from station 1 to 4 is mirrored in the increasing numbers of liths (Fig. 2); the patterns of stratification in temperature and lith counts are also strongly linked. However, it is difficult to determine whether the presence of the bloom caused the surface warming, deep cooling, and stable stratification of the water column or whether these physical characteristics were favorable for development of the bloom. Certainly the reduction in the light levels caused by the presence of the bloom would lead to cooler waters compared with the surrounding environmental water. Previous research⁹ and observations^{28,29} have shown that the presence of *E. huxleyi* causes surface heating. Although reflection increases (as corroborated by the enhanced water-leaving radiances), so does absorption in the near surface. Heating is proportional to scalar irradiance, and optical modeling⁹ shows that heating increases with coccolith concentration. The corresponding Advanced Very High Resolution Radiometer (AVHRR) satellite imagery shows that the warming occurs over the whole extent of the bloom.

B. Comparison of Measured Inherent Optical Properties

Figure 5 shows a direct comparison of the IOPs measured with the ac-9 and those calculated with the MSM as a function of wavelength. We derived the values by taking a mean value through the water column at each station and calculating the standard deviation. Figures 5(a) and 5(b) show that the absorption coefficient for both the MSM and the ac-9 are spectrally similar, with greater

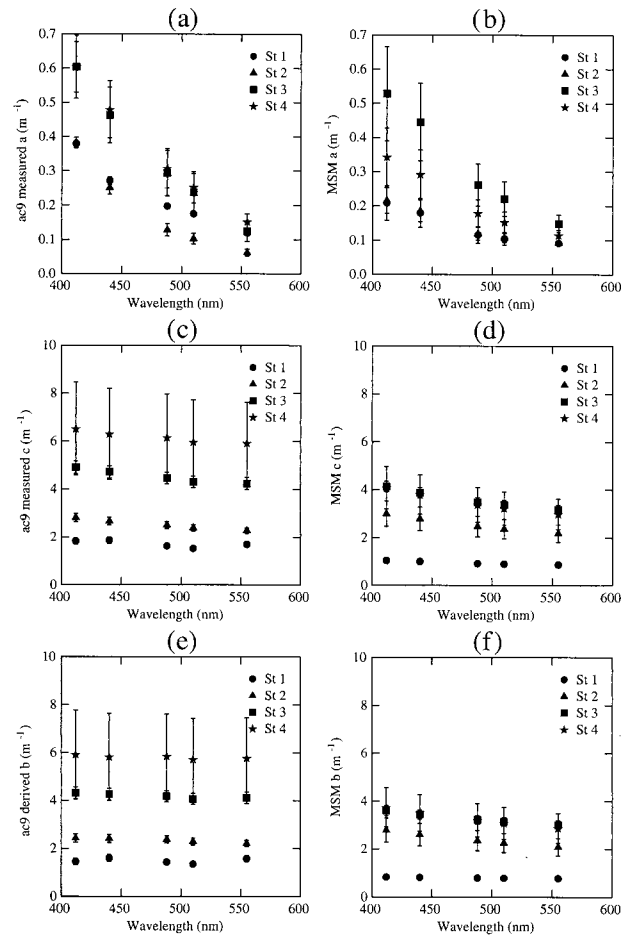


Fig. 5. Comparison of ac-9 and MSM values of (a), (b) absorption; (c), (d) attenuation; (e), (f) scattering as a function of wavelength at each station (St). Values are means over the water column; the attendant standard deviations are shown as error bars.

absorption occurring at shorter wavelengths. In Subsection 3(C) below, we show that when they are used as input into a radiative-transfer model the IOPs calculated with the MSM give a better representation of the in-water light field than do the IOPs measured with the ac-9. In the following discussion it is therefore assumed that the MSM is correct and that the ac-9 measured IOPs are in error. Figure 6 shows the difference between the IOPs measured with the ac-9 and those modeled by the MSM. Figure 6(a) shows that the ac-9 is measuring higher absorption than is predicted with the MSM, except at 555 nm. This difference is more pronounced at shorter wavelengths, which suggests that the scattering correction to the attenuation coefficient is incorrect or is based on assumptions that are invalid in such a strongly scattering medium. The correction assumes that there is some reference wavelength (715 nm for the ac-9 model) at which the absorption coefficient of particulate and dissolved materials is zero. It is further assumed that the shape of the volume scattering function is

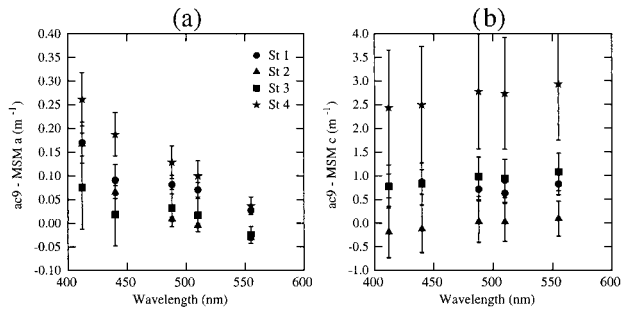


Fig. 6. Difference between the ac-9 measured and MSM values of (a) absorption and (b) attenuation at all stations (St). Data were derived from those in Fig. 5.

independent of wavelength. The correction technique is written as³⁰

$$a_t(\lambda) - a_w(\lambda) = a_m(\lambda) - \frac{a_{mts}(\lambda_{ref})}{[c_{mts}(\lambda_{ref}) - a_{mts}(\lambda_{ref})]} \times [c_m(\lambda) - a_m(\lambda)], \quad (13)$$

where the subscripts m , mts , t , and ref represent the measured, the measured temperature- and salinity-corrected, the total, and the reference coefficient values, respectively. To test this assumption we calculated the scattering correction to the attenuation coefficient at 715 and 676 nm for the ac-9 data. With such a narrow wavelength displacement and pure seawater absorption dominating, the difference between the two channels should be negligible. We tested this theory by using the following equation:

$$\epsilon = \frac{a_{mts}(\lambda_{ref})}{[c_{mts}(\lambda_{ref}) - a_{mts}(\lambda_{ref})]}. \quad (14)$$

We found that the average difference between $\epsilon(676 \text{ nm})$ and $\epsilon(715 \text{ nm})$ was 0.0134 ± 0.0059 over the four stations studied. If this error is considered to be inversely proportional to wavelength, then the correction to the absorption coefficient should be 0.104 ± 0.046 at 412 nm, which is comparable to the difference between the MSM–ac-9 difference shown in Fig. 6. However there is no physical reason to use this as a correction technique for the absorption coefficient.

The attenuation (c) measurements are limited by the acceptance angle (α) of the ac-9 (0.7°); i.e., any light that is scattered from 0 to 0.7° , is treated as unscattered, giving an underestimate of attenuation. The percentage error in the scattering (b) measurements can be approximated as follows:

$$b_e = \left[\frac{\int_0^\alpha \tilde{\beta}(\psi) \sin \psi d\psi}{\int_0^\pi \tilde{\beta}(\psi) \sin \psi d\psi} \right] \times 100\%. \quad (15)$$

Using the phase functions shown in Fig. 3 results in 2% and 10% errors for the Voss and the Petzold phase functions, respectively. However, these errors do

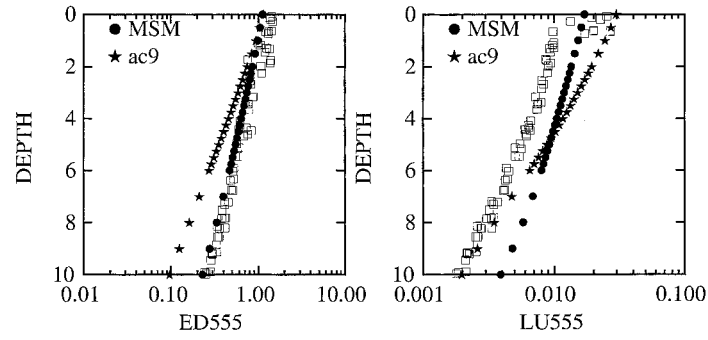
not account for the differences shown in Fig. 6(b), where the ac-9 attenuation measurements are 1–3 m^{-1} higher than those calculated by the MSM, instead of lower as predicted from the above discussion. However, Fig. 5(e) shows that the ac-9 calculated scattering coefficient is greater than the reciprocal of the path length (0.25 m) at stations 3 and 4. When $b \geq 4$, multiple scattering within the instrument becomes significant and the single-scattering approximation no longer holds. Possible ways to correct for attenuation (and consequently for absorption) in such a highly scattering medium would be to use a Monte Carlo ac-9 model to quantify multiple scattering effects or to measure the multiple scattering effect by using spheres with known values of b . The MSM and ac-9 values of b at stations 2–4 are consistent with the observation of the optics rig disappearing from view at a depth of $\sim 30 \text{ cm}$.

C. Optical Comparison

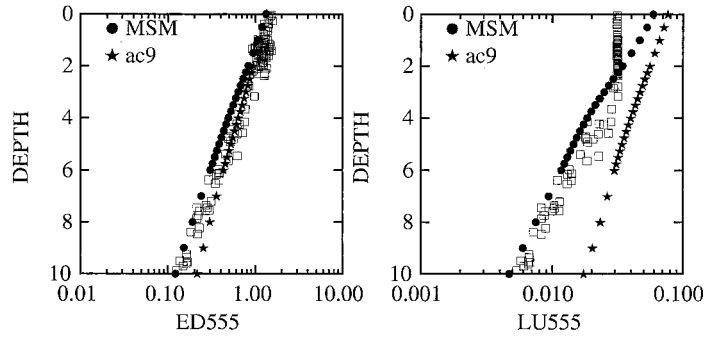
Figure 7 shows a comparison of E_d and L_u at 555 nm measured optically and modeled with the Hydrolight code with the MSM and ac-9 IOPs used as input. $L_u(555)$ is shown to saturate at stations 2–4, consistently with the extraordinary brightening of the surface layer observed within this bloom of *E. huxleyi*. This saturation hinders any retrieval of the surface layer radiance field, but L_{wn} can still be approximated by use of the data beneath the saturated layer and extrapolation of them to the surface by a log-linear regression. If the measured profiles are considered to be correct, the MSM gives the best approximation for $E_d(555)$ at all stations and for $L_u(555)$ at all stations except station 3. The differences between the MSM and ac-9 derived profiles can be illustrated by use of the diffuse attenuation coefficient, K_d . The spectral variations in this parameter at each station are shown in Fig. 8. There is very little difference between the MSM and the optically retrieved values of K_d . The average value of K_d across the spectrum derived with the MSM is within 1% of that determined from the optical measurements at stations 1, 2, and 4, whereas the ac-9 derived values are from 5% (station 2) to 76% (station 1) higher. Table 2 shows that the MSM gives better agreement across the spectrum, with a slope closer to unity and a greater amount of variance explained than the ac-9 derived data. Most of the deviation from unity for the MSM is a result of measurements at station 3.

Figure 9 shows a comparison of MSM, ac-9, optics, and SeaWiFS derived values of L_{wn} for the four stations. It shows that the four data sources generally agree better at 440 (443), 488 (490), and 510 than at 412 and 555 nm. The results for station 4 show that the *in situ* optics are a factor of 2 higher than the modeled and the SeaWiFS retrieved values of $L_{wn}(412)$ and $L_{wn}(555)$. We observed that at station 4 the sampling was carried out within 200 m of the edge of the bloom, raising issues concerning spatio-temporal variability and point representativity. The sampling at station 4 was carried out $\sim 2 \text{ h}$ later

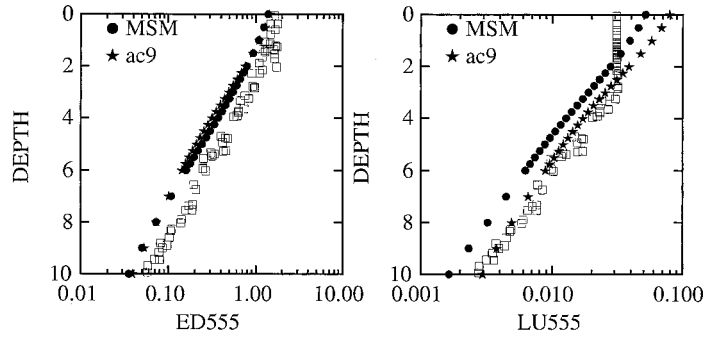
Station 1



Station 2



Station 3



Station 4

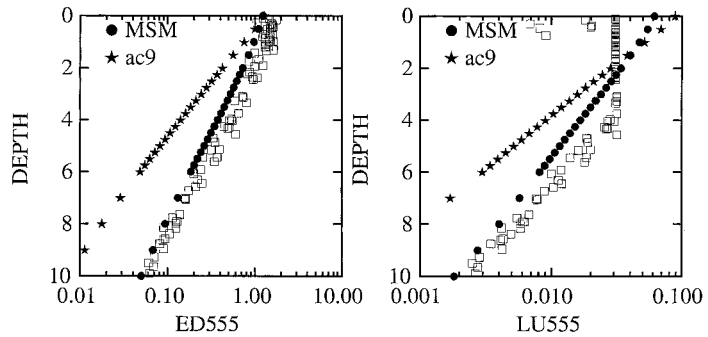


Fig. 7. Comparison of data modeled with the Hydrolight code with MSM and with ac-9 IOPs and of *in situ* measurements (open squares) of $L_u(555)$ and $E_d(555)$ at all four stations sampled on 30 July 1999.

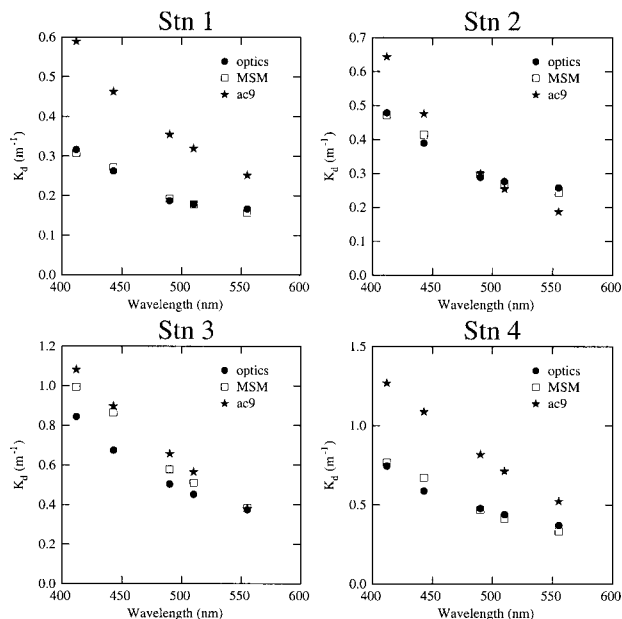


Fig. 8. Comparison of K_d measured with the *in situ* optics and that modeled with the MSM and ac-9 data. Stn, station.

than the SeaWiFS overpass. If part of the pixel lay outside the bloom, it would considerably lower the satellite-retrieved radiance and invalidate the assumption that the point optical measurement was representative of the $1.2 \text{ km} \times 1.2 \text{ km}$ pixel. Higher radiances are also subject to more spatial and temporal variability, so any small drift could cause differences between the optical measurements and the biological sampling carried out only 10 min later at the same point. It would certainly lead to differences between the *in situ* optics and the SeaWiFS retrievals. For optical studies of coccolithophore blooms one should therefore choose sampling locations at random on the largest measurement scale used (e.g., a SeaWiFS pixel) to overcome this problem of point representativity in high-reflectance regions. Only in this way can valid statistics be gathered to be compared with satellite measurements. Stations should not be chosen on the basis of selecting the so-called best high reflectance regions, except at larger scales.

Table 2 shows that the SeaWiFS retrieval across

Table 2. Results of the Regressions of MSM, ac-9, and SeaWiFS against *in situ* Optics for K_d and L_{wn} ^a

Method	K_d			L_{wn}		
	<i>m</i>	<i>c</i>	R^2	<i>m</i>	<i>c</i>	R^2
MSM	1.22	-0.07	0.97	1.07	-0.28	0.74
ac-9	1.50	-0.03	0.83	1.07	-0.23	0.49
SeaWiFS				1.00	0.19	0.79

^aRegressions are for K_d and L_{wn} at all wavelengths (412, 443, 490, 510, and 555 nm). Station 4 is omitted from the L_{wn} comparison. *m*, Slope; *c*, intercept. $N = 20$ for K_d and $N = 15$ for L_{wn} .

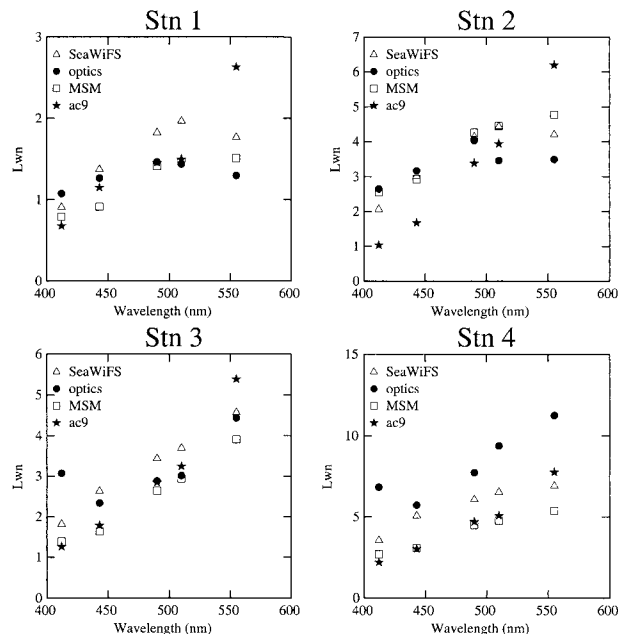


Fig. 9. Comparison of L_{wn} measured with *in situ* optics and SeaWiFS, and of L_{wn} modeled with MSM and ac-9 data. Stn, station.

the spectrum has a slope of regression against the *in situ* optics (omitting station 4) that is close to unity, which explains 79% of the variance. However, care must be taken in interpreting these results, as subtle spectral differences are masked. For example, at station 3 the SeaWiFS retrieved $L_{wn}(555)$ is within 4% of the optics but $L_{wn}(412)$ is 41% lower for SeaWiFS than the coincidental optics measurement. However, there are unresolved issues of calibration and atmospheric correction (possibly caused by absorbing aerosols) with the SeaWiFS 412-nm channel at the present, manifested in the large areas of negative retrievals of $L_{wn}(412)$ in coastal zones around the globe. As a caveat, the *in situ* optics calculated $L_{wn}(412)$ may be more accurate than $L_{wn}(555)$, as $L_{wn}(412)$ is saturated only for the top meter of the water column, compared with the top 4 m of the 555-nm profile. Table 2 shows that the MSM retrievals are closer to the *in situ* measurements than the ac-9 derived values. This is especially true for K_d but only marginally so for L_{wn} . Overall, therefore, within this coccolithophore bloom the MSM calculated light fields (both upwelling and downwelling)

Table 3. Comparison of Ratios of Apparent Optical Properties Calculated with the MSM and the THM Models and *in situ* Optics at 555 nm

Station	K_d		L_{wn}	
	MSM	THM	MSM	THM
1	0.95	1.10	1.16	0.94
2	0.94	0.90	1.37	0.94
3	1.04	0.86	0.88	0.71
4	0.90	0.81	0.48	0.37

give closer agreement with the *in situ* optics than those calculated from the ac-9 data.

D. Comparison of the MSM and a Coccolithophore IOP Model

We used the IOP equations described by Tyrrell *et al.*⁹ within a modified version of the Hydrolight radiative-transfer code. We ran the Tyrrell Hydrolight model (THM) at 555 nm to compare with the MSM. Rather than using coccolith numbers to calculate scattering, the THM model uses particulate inorganic carbon,³¹ i.e., the mass of CaCO₃. To obtain particulate inorganic carbon from the coccolith abundance we used a factor of 1.0 picograms of carbon per coccolith (pg C coccolith⁻¹), which is slightly greater than the value of ~0.8 pg C coccolith⁻¹ from a previous study of the western English Channel.²⁷ Table 3 shows the ratios of $L_{wn}(555)$ and $K_d(555)$ for both the THM and the MSM to the *in situ* optics. The MSM model predicts $K_d(555)$ to within 10% of the optics, whereas the THM model has errors of as much as 20%. The THM model gives closer agreement with the measured L_{wn} at stations 1 and 2; both models give poor performance at station 4, which has the highest coccolith concentration. The reason for this could be the steep decline in coccolith numbers (see Fig. 2) between the surface and 5-m depth coupled with the saturation of the $L_u(555)$ channel for the top 4 m of the water column (see Fig. 7). The reduction in the number of liths could lead to highly nonlinear behavior (in log space) of $L_u(555)$ in the top 4 m, which is difficult to quantify because of the channel saturation. This means that extrapolation of $L_u(555)$ to the surface leads to an overestimation of $L_{wn}(555)$.

4. Conclusions

In this paper we have shown that ac-9 measured absorption and attenuation are generally overestimated within a highly scattering medium such as a coccolithophore bloom. Two factors account for this overestimation. The first, the assumption that the scattering correction to the absorption measurement based on some reference wavelength is independent of wavelength, has been invalidated. The second is that multiple scattering ($b \geq 4 \text{ m}^{-1}$) corrupts the absorption measurements. Both of these factors render ac-9 measurements within such a highly scattering medium difficult to correct for.

When the inherent optical properties generated by the modified model of Sathyendranath *et al.* are used as input to the Hydrolight radiative transfer model and the apparent optical properties are calculated, the MSM gives K_d within 10% of that calculated with the *in situ* optics. This is an improvement over the previously published THM model, which gives a 10–20% difference in the calculated K_d for the same data set. The upwelling radiance at 555 nm is not modeled so well as the downwelling irradiance for this data set. There can be as much as a factor-of-2 difference between the measured and the calculated L_{wn} . This difference could be explained by the mod-

el's producing better estimates of absorption than of scattering, which in turn is strongly dependent on the phase function used. The phase function itself is difficult to characterize because of the size, shape, and composition of the coccoliths. There may even be variation in the form of the phase function from bloom to bloom. However, we have shown in this paper that the MSM produces IOPs that give an improvement over previously published models and give results that are comparable with those for the observed light field when it is used as an input into the Hydrolight model.

We thank the crew and support staff of the RV Squilla for their invaluable assistance during the sampling campaign and Curtis Mobley for making Hydrolight v3.0 code freely available. We also thank Howard Gordon for providing the coccolithophore phase function, Denise Cummings for carrying out the high-performance liquid chromatography analysis, Derek Harbour for doing the coccolithophore counts, and Glen Tarran for providing the flow cytometry results. We thank the SeaWiFS Project (code 970.2) and the Dundee Satellite Receiving Station for reception and transmission of SeaWiFS data to the Plymouth Marine Laboratory. This research has been carried out as part of the Plymouth Marine Research Laboratory Microbially Driven Biogeochemical Process, Exchanges, and Controls program.

References

1. J. L. Mueller and R. W. Austin, *Ocean Optics Protocols for SeaWiFS Validation*, rev. 1, Vol. 25 of SeaWiFS Tech. Rep. Series, S. B. Hooker and E. Firestone, eds., NASA Tech. Memo **104566** (1995).
2. H. R. Gordon and D. K. Clark, "Clear water radiances for atmospheric correction for Coastal Zone Color Scanner imagery," *Appl. Opt.* **22**, 3929–3931 (1981).
3. H. Neckel and D. Labs, "The solar radiation between 3300 and 12500 Å," *Solar Physics* **90**, 205–258 (1984).
4. R. C. Smith and K. S. Baker, "Optical properties of the clearest natural waters (200–800 nm)," *Appl. Opt.* **20**, 177–184 (1981).
5. C. Moore, "In situ, biochemical, oceanic, optical meters," *Sea Technol.* **35**, 10–16 (1994).
6. R. M. Pope and E. S. Fry, "Absorption spectrum (380–700 nm) of pure water. II. Integrating cavity measurements," *Appl. Opt.* **36**, 8710–8722 (1997).
7. L. H. Kou, D. Labrie, and P. Chylek, "Refractive-indexes of water and ice in the 0.65- μm to 2.5- μm spectral range," *Appl. Opt.* **32**, 3531–3540 (1993).
8. H. Buiteveld, J. H. M. Hakvoort, and M. Donze, "The optical properties of pure water," in *Ocean Optics XII*, J. Jaffe, ed., Proc. SPIE **2258**, 174–183 (1994).
9. T. Tyrrell, P. M. Holligan, and C. D. Mobley, "Optical impacts of oceanic coccolithophore blooms," *J. Geophys. Res.* **104**, 3223–3241 (1999).
10. S. G. Ackleson, W. M. Balch, and P. M. Holligan, "Response of water-leaving radiance to particulate calcite and chlorophyll *a* concentrations: a model for Gulf of Maine coccolithophore blooms," *J. Geophys. Res.* **99**, 7483–7499 (1994).
11. S. Sathyendranath, G. Cota, V. Stuart, H. Maass, and T. Platt, "Remote sensing of phytoplankton pigments: a comparison of empirical and theoretical approaches," *Int. J. Remote Sens.* **22**, 249–273 (2001).
12. A. Morel, "Optical properties of pure seawater," in *Optical*

- Aspects of Oceanography*, N. G. Jerlov and E. S. Nielsen, eds. (Academic, New York, 1974), pp. 1–24.
13. H. R. Gordon, G. C. Boynton, W. M. Balch, S. B. Groom, D. S. Harbour, and T. J. Smyth, "Retrieval of coccolithophore calcite concentration from SeaWiFS imagery," *Geophys. Res. Lett.* **28**, 1587–1590 (2001).
 14. K. J. Voss, W. M. Balch, and K. A. Kilpatrick, "Scattering and attenuation properties of *Emiliana huxleyi* cells and their detached coccoliths," *Limnol. Oceanogr.* **43**, 870–876 (1998).
 15. C. D. Mobley, *Light and Water: Radiative Transfer in Natural Waters* (Academic, San Diego, Calif., 1994), Chap. 3, table 3.10.
 16. W. M. Balch, K. A. Kilpatrick, P. M. Holligan, D. S. Harbour, and E. Fernandez, "The 1991 coccolithophore bloom in the central North Atlantic. 2. Relating optics to coccolith concentration," *Limnol. Oceanogr.* **41**, 1684–1696 (1996).
 17. J. E. O'Reilly, S. Maritorena, B. G. Mitchell, D. A. Siegel, K. L. Carder, S. A. Garver, M. Kahru, and C. McClain, "Ocean color chlorophyll algorithms for SeaWiFS," *J. Geophys. Res.* **103**, 24,937–24,953 (1998).
 18. R. G. Barlow, D. G. Cummings, and S. W. Gibb, "Improved resolution of mono- and divinyl chlorophylls a and b and zeaxanthin and lutein in phytoplankton extracts using reverse phase C-8 HPLC," *Marine Ecol. Prog. Ser.* **161**, 303–307 (1997).
 19. H. R. Gordon and T. Du, "Light scattering by nonspherical particles: application to coccoliths detached from *Emiliana huxleyi*," *Limnol. Oceanogr.* **46**, 1438–1454 (2001).
 20. H. Gordon, Department of Physics, University of Miami, Coral Gables, Fla. 33124 (personal communication, 2001).
 21. K. Voss, Department of Physics, University of Miami, Coral Gables, Fla. 33124 (personal communication, 2001).
 22. C. D. Mobley, "HYDROLIGHT 3.0 User's Guide" (SRI International, Menlo Park, Calif., 1995).
 23. W. W. Gregg and K. L. Carder, "A simple spectral solar irradiance model for cloudless maritime atmospheres," *Limnol. Oceanogr.* **35**, 1657–1675 (1990).
 24. M. J. W. Veldhuis and G. Kraay, "Application of flow cytometry in marine phytoplankton research: current applications and future perspectives," *Scientia Marina* **64**, 121–134 (2000).
 25. G. Taran, Plymouth Marine Laboratory, Prospect Place, Plymouth, PL13DH, U.K. (personal communication, 2001).
 26. D. Harbour, Sir Alistair Hardy Foundation for Ocean Science, Plymouth, U.K. (personal communication, 2001).
 27. G. Garcia-Soto, E. Fernandez, R. D. Pingree, and D. S. Harbour, "Evolution and structure of a shelf coccolithophore bloom in the Western English Channel," *J. Plankton Res.* **17**, 2011–2036 (1995).
 28. P. Holligan, M. Voiller, D. S. Harbour, P. Camus, and M. Champagne-Phillippe, "Satellite and ship studies of coccolithophore production along a continental shelf edge," *Nature* **304**, 339–342 (1983).
 29. P. M. Holligan, E. Fernandez, J. Aiken, W. M. Balch, P. Boyd, P. H. Burkill, M. Finch, S. B. Groom, G. Malin, K. Muller, D. A. Purdie, C. Robinson, C. C. Trees, S. M. Turner, and P. Vanderwal, "A biogeochemical study of the coccolithophore *Emiliana huxleyi* in the North Atlantic," *Global Biogeochem. Cycles* **7**, 879–900 (1993).
 30. J. R. V. Zaneveld and R. Bartz, "Beam attenuation and absorption meters," in *Ocean Optics VII*, J. S. Jaffe, ed., Proc. SPIE **489**, 318–342 (1984).
 31. W. M. Balch, K. A. Kilpatrick, and C. C. Trees, "The 1991 coccolithophore bloom in the central North Atlantic. 1. Optical properties and factors affecting their distribution," *Limnol. Oceanogr.* **41**, 1669–1683 (1996).